HHS Public Access

Author manuscript

*Neuroimage*. Author manuscript; available in PMC 2020 December 15.

Published in final edited form as:

*Neuroimage*. 2020 November 15; 222: 117278. doi:10.1016/j.neuroimage.2020.117278.

# Detection of functional networks within white matter using independent component analysis

**Yali Huang**[a], **Yang Yang**[b], **Lei Hao**[a], **Xuefang Hu**[a], **Peiguang Wang**[a,c,*], **Zhaohua Ding**[d,e], **Jia-Hong Gao**[b,f,g], **John C. Gore**[d,h,i,j,k,**]

[a]College of Electronics and Information Engineering, Hebei University, Baoding 071002, China

[b]Center for MRI Research, Academy for Advanced Interdisciplinary Studies, Peking University, Beijing 100871, China

[c]College of Mathematics and Information Science, Hebei University, Baoding 071002, China

[d]Vanderbilt University Institute of Imaging Science, Vanderbilt University, Nashville, TN 37232, United States

[e]Department of Electrical Engineering and Computer Science, Vanderbilt University, Nashville, TN 37232, United States

[f]Beijing City Key Lab for Medical Physics and Engineering, Institute of Heavy Ion Physics, School of Physics, Peking University, Beijing 100871, China

[g]McGovern Institute for Brain Research, Peking University, Beijing 100871, China

[h]Department of Radiology and Radiological Sciences, Vanderbilt University Medical Center, Nashville, TN 37232, United States

[i]Department of Biomedical Engineering, Vanderbilt University, Nashville, TN 37232, United States

[j]Department of Molecular Physiology and Biophysics, Vanderbilt University, Nashville, TN 37232, United States

[k]Department of Physics and Astronomy, Vanderbilt University, Nashville, TN 37232, United States

## Abstract

Spontaneous fluctuations in MRI signals from gray matter (GM) in the brain are interpreted as originating from variations in neural activity, and their inter-regional correlations may be analyzed to reveal functional connectivity. However, most studies of intrinsic neuronal activity have ignored the spontaneous fluctuations that also arise in white matter (WM). In this work, we explore



*Corresponding author at: College of Electronics and Information Engineering, Hebei University, Baoding 071002, China. pgwang@hbu.edu.cn (P. Wang). **Corresponding author at: Vanderbilt University Institute of Imaging Science, 1161 21st Ave South, Nashville, TN 37212, USA. john.gore@vanderbilt.edu (J.C. Gore).

CRediT authorship contribution statement

**Yali Huang:** Methodology, Software, Formal analysis, Writing - original draft. **Yang Yang:** Data curation. **Lei Hao:** Software, Visualization. **Xuefang Hu:** Software, Visualization. **Peiguang Wang:** Project administration. **Zhaohua Ding:** Project administration, Writing - review & editing. **Jia-Hong Gao:** Project administration. **John C. Gore:** Project administration, Writing - review & editing.

Supplementary materials

Supplementary material associated with this article can be found, in the online version, at doi:10.1016/j.neuroimage.2020.117278.

spontaneous fluctuations in resting state MRI signals in WM based on spatial independent component analyses (ICA), a data-driven approach that separates signals into independent sources without making specific modeling assumptions. ICA has become widely accepted as a valuable approach for identifying functional connectivity within cortex but has been rarely applied to derive equivalent structures within WM. Here, BOLD signal changes in WM of a group of subjects performing motor tasks were first detected using ICA, and a spatial component whose time course was consistent with the task was found, demonstrating the analysis is sensitive to evoked BOLD signals in WM. Secondly, multiple spatial components were derived by applying ICA to identify those voxels in WM whose MRI signals showed similar temporal behaviors in a resting state. These functionally-related structures are grossly symmetric and coincide with corresponding tracts identified from diffusion MRI. Finally, functional connectivity was quantified by calculating correlations between pairs of structures to explore the synchronicity of resting state BOLD signals across WM regions, and the experimental results revealed that there exist two distinct groupings of functional correlations in WM tracts at rest. Our study provides further insights into the nature of activation patterns, functional responses and connectivity in WM, and support previous suggestions that BOLD signals in WM show similarities with cortical activations and are characterized by distinct underlying structures in tasks and at rest.

**Keywords**

White matter fMRI; Functional activation; Functional structure; Functional connectivity; Independent component analysis

## 1. Introduction

Functional MRI (fMRI) has been widely used to assess the functional roles of localized brain regions based on detecting changes in neural activity in gray matter (GM) via blood oxygenation level dependent (BOLD) effects, and fMRI methods have been extended to be able to measure functional connectivity between regions (Ogawa et al., 1990; Biswal et al., 1995; Fox and Raichle, 2007; Gonzalez-Castillo et al., 2014). Much attention has been focused on resting-state networks (RSN) which may be delineated by detecting temporal correlations between the spontaneous fluctuations in BOLD signals from different regions, which are then assumed to exhibit functional connectivity (Fox and Raichle, 2007; Gonzalez-Castillo et al., 2014; Zhang and Raichle, 2010; Lee et al., 2013). Several temporally coherent RSNs that subserve critical functions including vision, hearing, language and attention have been delineated in GM by resting state fMRI studies (Biswal et al., 1995; Fox and Greicius, 2010), while the default-mode network (DMN) includes a set of GM regions preferentially active when individuals are left undisturbed by the external environment (Raichle et al., 2001; Buckner et al., 2008). The DMN is not only robustly detectable in the absence of a particular task, but also is of particular interest because it is altered in a number of different neurological or psychiatric disorders (Greicius, 2008). White matter (WM) comprises over half the brain volume and serves to connect and communicate information between different nodes within functional networks in GM. In most reports of fMRI applications there is little mention of BOLD signal changes in WM, and whether there are robustly detectable correlations of signals from within WM that are related to specific

functions remains unclear. However, a few recent studies have reported robust activity-related BOLD signals in WM as well as resting state correlations between specific WM tracts or with parcellated cortical volumes (Ding et al., 2013; Ding et al., 2018; Marussich et al., 2017; Peer et al., 2017). The origins of these functional signals in WM have not been established, but equally they have not been rigorously examined using the same methods as have been applied to GM.

Diffusion tensor imaging (DTI) provides a way to delineate nerve fiber tracts and analyze structural connectivity in WM, but DTI does not reveal information about WM function (Basser et al., 1994). Whether BOLD signals in WM are related to intrinsic neural activity, or are the result of vascular changes in neighboring cortex, or some other processes, remains unclear, but efforts have been made by several groups to detect and evaluate BOLD signals in WM. In fact, a growing number of studies have shown the feasibility of reliably detecting functional activation and connectivity by fMRI in WM (Ding et al., 2013, 2018, 2016; Gore et al., 2019; Grajauskas et al., 2019). For instance, Mazerolle et al. reported functional activation in the isthmus of the corpus callosum by using a Sperry task and high field imaging (4 T) (Mazerolle et al., 2008). Gawryluk et al. replicated WM activation in the anterior corpus callosum using an interhemispheric transfer task and asymmetric spin echo (ASE) spiral sequence at 4 T (Gawryluk et al., 2009). These studies reported activation in different areas of the corpus callosum, and both were functionally consistent with the tasks. Gawryluk et al. also used a specialized ASE spiral sequence and a motor task to elicit WM activation in the posterior limb of the internal capsule (Gawryluk et al., 2011). Meanwhile, Fabri and Polonara reported that BOLD effects can be evoked in the corpus callosum by peripheral sensory stimulation or motor tasks, and that the corpus callosum activation foci had locations consistent with the sensory or motor stimulus applied (Fabri and Polonara, 2013). In our own reports, we have demonstrated with various stimuli that relevant WM tracts show task-specific BOLD changes (Ding et al., 2018; Wu et al., 2017; Huang et al., 2018; Li et al., 2019).

Most previous studies of functional BOLD changes in WM are based on evoked responses to tasks or stimulation prescribed with well-defined timings, which facilitates the detection of WM activation by conventional methods, e.g., by frequency spectrum analysis or convolution approaches. However, these methods are generally not applicable to other situations in which task or stimulus timing is not known a priori. During resting state acquisitions, no explicit timing of spontaneous neural events is available. Peer et al. (2017) used a K-means clustering analysis of resting state signals in WM to identify a set of correlated voxels corresponding to distinct networks but otherwise there have been only sparse attempts to use data-driven analyses of whole brain resting state data, as have been used for GM, to identify potential functional networks in WM. Notably, Marussich et al. (2017) used independent components analysis (ICA) to derive spatially independent patterns in 11 subjects that appeared to reorganize during natural vision. Here we have employed spatial ICA to define a primary set of independent networks of co-activation patterns in BOLD signals across the entire WM in the brains of large sets of normal subjects.

Spatial ICA requires no prior regional seed definitions and separates data into components that are maximally independent in a statistical sense (Calhoun et al., 2001, 2009). Each

independent component (IC) represents a major co-activation mode within the original data. ICA assumes that the observed data are made up of statistically independent components that are not separable experimentally and are combined by an unknown linear mixing process. It attempts to separate the observed data into independent sources by finding a linear transformation that provides a set of maximally independent components, but without making specific modeling assumptions (Calhoun et al., 2001). ICA has been widely used to explore intrinsic neuronal activity and connectivity in the cortex (Calhoun et al., 2009; McKeown et al., 1998; Biswal and Ulmer, 1999), and to identify several networks including vision, default mode, cerebellar, sensorimotor, auditory, motor, executive control and frontoparietal networks (Beckmann et al., 2005; Smith et al., 2009, 2012). Here we apply similar ICA techniques to detect and identify patterns of BOLD signals in WM.

The main purposes of this work are to detect and identify patterns of synchronized, spontaneous fluctuations of BOLD signals in WM in a resting state using the well-established ICA method, and to use the results to derive structures which share BOLD-signal co-activation and provide the basis for further analyses of functional connectivity within the brain. By examining data from a large set of standardized scans, this goal would establish objectively the principal RSN that are reliably found in WM. We first applied ICA to evaluate WM signals produced during a simple block-design motor task to validate the effectiveness of ICA for detecting relevant WM BOLD changes with no prior information. Then we use ICA to derive resting state functional structures in WM from a set of images obtained by the China Human Connectome Project (CHCP). The reproducibility of the results is demonstrated by applying the same analyses to a second, larger, independent cohort of images from the Human Connectome Project (HCP) (Van Essen et al., 2013). Lastly, we further explore functional connectivity within and between the functional structures in WM derived from the CHCP data. Our results demonstrate (i) that WM functional activation elicited during a motor task is detectable using ICA; WM areas showing BOLD activation by ICA were adjacent to corresponding GM motor areas; (ii) functional structures identified by ICA are consistent with WM tracts derived from DTI (Mori et al., 2008); (iii) functional connectivity within identified WM ICA components is indicative of synchronized temporal fluctuations in BOLD signals within individual WM tracts at rest (Shine et al., 2019); (iv) several pairs of ICA components showed correlated time courses. This study provides additional insights into the nature of functional activation, structures and connectivity in cerebral WM, and confirms that BOLD signals in WM are organized in a manner that they potentially reveal important functional relationships between regions.

## 2. Methods

### 2.1. Subjects and image acquisitions

#### 2.1.1. *Subjects undertaking a motor task* (data acquired at Vanderbilt University)—

The task data analyzed were part of the datasets reported in a previous study (Ding et al., 2018). 12 healthy right handed volunteers (mean age: 27.8 ± 4.8 years; range: 23–37 years), with no history of neurological, psychiatric or medical conditions as

determined by interview, participated in a protocol approved by the Institutional Review Board at Vanderbilt University, Nashville, TN.

The motor task was prescribed in a block design format. Each subject underwent two fMRI acquisitions with different conditions, one session with left finger movements, and the other with right finger movements. The subjects fixed on a cross sign projected on the middle of a screen in their field of view when there were no tasks. Motor tasks started with 30 seconds of finger movement, in which subjects successively tapped each finger of the hand indicated by an arrow, followed by 30 seconds of no finger movement, for a total of seven blocks for each condition. Each imaging run had a time duration of 435 seconds. Subject head motions were minimized by restricting pads placed within the head coil.

Functional and structural images of the brain were acquired with a 3 T Philips Achieva CX scanner (Philips Healthcare, Inc., Best, Netherlands) using a 32-channel head coil at the Vanderbilt University Institute of Imaging Science. BOLD-sensitive functional images were obtained using a single shot $T_2$*-weighted gradient echo (GE), echo planar imaging (EPI) sequence (TR = 3000 ms, TE = 45 ms, matrix size = 80 × 80, FOV = 24 × 24 $cm^2$, 43 axial slices each 3 mm thick, and 145 volumes). High resolution $T_1$-weighted images were acquired using a multi-shot, 3D $T_1$-weighted GE sequence (1 × 1 × 1 $mm^3$ nominal resolution).

**2.1.2. *Subjects in a resting state* (data acquired at Peking University)—**The data used in this analysis were obtained from the CHCP. Thirty healthy volunteers (22 ± 2 years old, range: 19–27 years, 16 females) participated in this study in accordance with a protocol approved by the Institutional Review Board at Peking University. Each subject underwent two fMRI sessions with eyes-open in a resting state (we used only the data of the first session). Functional and structural images of the brain were acquired with a 3 T Siemens Prisma scanner using a 64-channel head coil at Peking University. BOLD-sensitive resting state functional images were obtained using a multi-shot $T_2$*-weighted GE, EPI sequence (TR = 710 ms, TE = 30 ms, matrix size = 106 × 106, flip angle = 54°, FOV = 21.2 × 21.2 $cm^2$, 72 axial slices each 2 mm thick, and 634 volumes). High resolution $T_1$-weighted images were acquired using a 3D GE sequence (0.8 × 0.8 × 0.8 $mm^3$ nominal resolution, TR/TE = 2400/2.22 ms, flip angle = 8°).

**2.1.3. *Subjects in a resting state* (data acquired by the Human Connectome Project)—**To examine reproducibility and perform additional analyses, we used data from the HCP, which were acquired on a customized Siemens 3 T “Connectome Skyra” using a 32-channel Siemens receive head coil. To minimize WM signal contamination from nearby GM, unprocessed fMRI data were used from 100 participants (age range: 22–35 years; 50 females). For each participant, BOLD resting state data were acquired using multiband gradient echo planar imaging. The following parameters were used for data acquisition: TR = 720 ms, TE = 33.1 ms, matrix size = 104 × 90, flip angle = 52°, FOV = 20.8 × 18.0 $cm^2$, 72 axial slices each 2 mm thick with left-right encoding, and 1200 volumes. High resolution $T_1$-weighted images were acquired using a 3D GE sequence (0.7 × 0.7 × 0.7 $mm^3$ nominal resolution, TR/TE = 2400/2.14 ms, flip angle = 8°).

### 2.2. Data preprocessing

The Vanderbilt University data were preprocessed using SPM12 (http://www.fil.ion.ucl.ac.uk/spm). First, the fMRI data were corrected for intra-volume acquisition time differences (module *slice timing*), and inter-volume head displacements (module *realign*). Head motions of all subjects were checked (< 2mm in translation or < 2° in rotation). Second, $T_1$ structural images of each subject were segmented into WM, GM, and cerebrospinal fluid (CSF) (module *segment*). Third, the segmented images, as well as the $T_1$ images, were co-registered to the mean coordinates of the fMRI data (module *co-register*). Fourth, all the resulting images were normalized into MNI (Montreal Neurological Institute) space (module *normalize*). Lastly, the fMRI data were segmented into WM and GM volumes based on the $T_1$ segmentation. To minimize potential partial volume effects from nearby structures, the WM volume was confined within a thresholded $T_1$ WM segment ($>0.8$), and spatial smoothing with a 4 mm full-width at half maximum (FWHM) Gaussian kernel was performed separately within the WM.

CHCP and HCP resting state data were processed in the same way as above, except slice timing corrections were not performed as TR was only 0.71 (CHCP) or 0.72 s (HCP). It should be noted that we didn't remove the mean of the time series from the fMRI data.

### 2.3. Group independent component analysis

ICA is based on the assumption that observed data are made up of independent components (source signals, which are not separately observable, are statistically independent and non-Gaussian in their properties), that have been combined using an unknown, but linear, mixing process. ICA was originally developed for blind source separation or the cocktail party problem, in which many people may be speaking simultaneously and ICA can successfully separate the contributions of each speaker (Bell and Sejnowski, 1995). The underlying model can be expressed in matrix form as: $\mathbf{X} = \mathbf{MS}$, where $\mathbf{X}$ is the observed T-by-V data (for fMRI data, T is the number of time points and V is the number of voxels); $\mathbf{S}$ denotes the source signals, and $\mathbf{M}$ is an unknown mixing matrix. The goal of ICA is to estimate an unmixing matrix $\mathbf{W}$, such that $\hat{\mathbf{S}}$ given by $\hat{\mathbf{S}} = \mathbf{WX}$ is a good approximation to the "true" source $\mathbf{S}$. In contrast to general linear models (GLM) that require the user to parameterize the data, a principal advantage of ICA is that it can characterize the observed mixture data without making specific modeling assumptions (Calhoun et al., 2001).

Typical fMRI data may include spontaneous (resting state) fluctuations, task-related activity signals, physiological noise signals (e.g. from heart beat and breathing), motion-related effects and variations caused by the MRI equipment. ICA may be used to separate fMRI data into either spatially or temporally independent sources via spatial ICA (McKeown et al., 1998) and temporal ICA (Biswal and Ulmer, 1999) analyses. Either independence of spatial maps or of time courses can be used to separate signal variations. ICA works well in both situations when appropriate assumptions are met (Calhoun et al., 2001; McKeown et al., 1998), and has been increasingly used to discover hidden spatiotemporal structure or features contained within fMRI data (Calhoun et al., 2009).

In this study, the preprocessed data were decomposed into independent components (ICs) using spatial ICA in which each component identifies patterns of voxels within WM that share a time-varying pattern of co-activation. Task and rest data were analyzed independently using the Group ICA of fMRI toolbox (GIFT) (http://mialab.mrn.org/software/gift).

The task-related and resting-state data were both analyzed using the same procedure. The workflow of an ICA analysis is summarized as follows: the dimensions of each subject's data were first reduced using principal component analysis (PCA); then the reduced data from all subjects were concatenated in the temporal dimension to form one set of data to be further reduced using PCA; lastly, the reduced data were fed into ICA and analyzed with the Infomax algorithm, which is well suited for spatial ICA analysis (Petersen et al., 2000), and the group ICs were obtained. The averaged spatial map for each group IC was converted to Z standard scores and thresholded at $Z > 2$ for display. Voxels with Z-scores greater than the threshold were considered to be the active voxels (McKeown et al., 1998). Once the aggregate components were estimated, the unmixing matrix was obtained. GICA based back-reconstruction methods use the aggregate components of ICA and the results from the data reduction step to compute the individual subject components, whereas a spatial-temporal regression approach uses aggregate components and the original data to reconstruct individual subject components (Calhoun et al., 2001).

For analyzing the motor task data, there are two data reduction steps: first, the data were reduced into 21 principal components, and then the aggregate data were reduced to 14 principal components; lastly the reduced data were fed into the ICA algorithm to obtain the aggregate components. We tried different numbers of components, and when the fMRI data are decomposed into 14 independent components, the time course of one specific spatial map best fit the stimulus signal waveform. In addition, the number of components estimated from all subject's data using the GIFT toolbox is 14.5. Therefore a 14-order ICA was implemented for the task dada.

For the resting-state data, we evaluated decompositions into different numbers of components (from 16 to 50). Previous studies have demonstrated that higher-order models may provide more specific components that correspond to known anatomical and functional segmentations (Smith et al., 2009). In the data reduction steps used here, each subject's data are reduced, and the principal component numbers are set to 1.5 times the number of final components. Secondly, the subjects are then concatenated into one group and subjected to another data reduction step to reach the final number of principal components. Note that the numbers of components for the resting state data are different from the task data but they were analyzed using the same ICA procedure.

We separate signals from artifacts in independent components using two approaches. First, we apply ICA with different orders of decomposition (16–50 components), and retain those components that consistently appear. In the case of obvious artifacts, the components are excluded by visual inspection. Second, the spatial maps from ICA decompositions are compared with WM tracts in the JHU atlas using MRIcron software (http://

www.mricro.com). We assume that if the peak activation coordinate of a component in the spatial maps is near the skeleton of a WM tract, it is more likely to be a signal from WM.

To evaluate the functional connectivity (FC) between components within WM, correlations between the time courses from pairs of WM structures were estimated by calculating Pearson's correlation coefficients. To do this, two steps of preprocessing were applied to the time series of each IC, including (i) six head-motion parameters were regressed out of the time series; (ii) the time courses were low pass filtered with a frequency cutoff of 0.1 Hz. Then we computed correlations between ICs for each subject, and FC was computed as the mean FC across all subjects.

To confirm the reliability of our methods, we also applied ICA to the segmented GM regions alone. It should be noted that spatial smoothing with a larger scale FWHM Gaussian kernel should be adopted to the segmented GM, for the segmented cortical surface is only ≈ 2–4 mm thick, which is so thin that the group mask obtained by coregistering multiple individuals may retain little tissue and fail to obtain the expected results. In our study the segmented GM (thresholded at 0.8) masks were smoothed with an 8 mm FWHM Gaussian kernel prior to applying the same ICA methods as for WM.

## 3. Results

### 3.1. Functional activations in white matter evoked by motor task

To detect the IC which matches the stimulus, we compared the mean time course of each spatial map with the stimulus signal (the motor task waveform). Among the 14 ICs obtained from the WM fMRI data with left finger movement, the time course of IC #4 was visually identified to be most similar to the stimulus signal, so IC #4 was identified as the activated IC corresponding to the stimulus. The spatial map and the coordinate of the peak activations of IC #4 are presented in Fig. 1 a (upper left). Here, to display voxels contributing most strongly to a specific component map, ICA spatial maps were scaled to Z standard scores and thresholded at $Z > 2$ ($p < 0.05$). More detailed distributions of IC #4 are presented in Fig. 1 b, which shows a superposition of axial slices from −40 to 58 onto the MNI 152 standard template. It can be seen that there is distinct lateralization of these spatial maps, with larger WM activated regions located in the contralateral bundles. The peak activation regions are located in the corticospinal tract (CST) (defined by Bürgel et al., 2006) and in the middle cerebellar peduncle (MCP) for the contralateral and ipsilateral hemisphere, respectively.

To compare the functional response between WM and GM, the same ICA algorithm as for WM was applied to the segmented GM data. The maps of GM signal changes corresponding to the stimulus and the peak activation coordinates are shown in Fig. 1 a (upper right). To compare the responses of white and gray matter, the mean time series of the WM and GM activation maps (IC #4 in WM and IC #2 in GM) across 12 subjects (one session each) are presented in Fig. 1 a (lower). To show the results clearly, the mean fMRI signals within the ICs were removed. It can be seen that (i) the time courses of signal variations in the WM are similar to those in the activated GM, both of which are consistent with the stimulus; (ii) signal changes in GM are much greater than in WM, with stimulus-induced signal increases

from the baseline of 2.45% and 0.78%, respectively for the GM and WM; (iii) there is little difference in time delay between WM and GM.

We also compared the signal-to-noise ratio (SNR) between GM and WM in the two selected ICs. The SNR was computed as the ratio of the mean to the standard deviation of the response time series averaged over the 12 subjects studied. Specifically, the spatial map corresponding to each of the ICs was first identified in the GIFT output for each subject, from which the mean time series of the spatial map was computed. Then the mean response time series across the 12 subjects was obtained. The mean BOLD signal was found to be $2.44 \times 10^{5}$ and $1.86 \times 10^{5}$ (arbitrary units) for GM and WM, respectively, and the standard deviation of the mean response time series was $4.37 \times 10^{3}$ and $2.28 \times 10^{3}$ for GM and WM, respectively, which yields an SNR of 55.77 and 81.63 respectively for GM and WM. The coefficients of variations, defined as the inverse of SNR, are 0.018 and 0.012 for GM and WM, respectively. These measures are consistent with our earlier report (Huang et al., 2018). Of note, the observation that GM has a higher standard deviation may be due to the greater physiological noise in regions of higher vascular density.

Spatial maps and time courses shown in Fig. 1 represent group components (averaged across 12 subjects) with left finger movement. Similar results from right finger movement are presented in supplementary materials (Fig. S1) where the time course of IC #5 is visually nearly identical to the stimulus waveform. It is appreciated that, similar to the left finger movement above, peak activations appear in the contralateral CST and in the ipsilateral MCP. However, there is also a noticeable difference between the left and right finger tasks: while the former elicits peak activation in the cerebrum (CST), the latter evokes peak activation in the cerebellum (MCP).

### 3.2. Functional structures in white matter in a resting state

We applied ICA to the CHCP and HCP datasets using identical procedures and parameters to derive functional structures in WM from resting state data, and also explored their reproducibility across different studies. To evaluate the impact of the number of components on the ICA results, it was varied from 16 to 50, and we observed that several components were very similar between the two separate datasets. The most reproducible components are presented in Fig. 2 (the first and second columns corresponding to the results of the CHCP and HCP data, respectively), which correspond closely with WM tracts in the JHU atlas. To find the correspondence between these components and specific tracts, we first determined the location of the peak value for each component, and then established which spatial domain of the JHU WM atlas it falls in using the software MRIcron.

Each component from the ICA decomposition represents voxels showing correlated patterns of BOLD signals over time, which may be interpreted as a functional structure. Four representative functional structures are shown in Fig. 2 : MCP, posterior thalamic radiation (PTR) (including optic radiation, OR), splenium of corpus callosum (SCC), and CST. It should be noted that the PTR results in the HCP data may be further decomposed into two ICs if the number of components $>= 30$, as shown in the third column of Fig. 2, but spatial maps of MCP, SCC and CST are consistent from 24 to 50 dimensional ICA decompositions, as shown in the supplementary materials (Fig. S2).

We also compared the above functional structures (MCP, SCC and PTRderived from CHCP) with the JHU atlas, as shown in Fig. 3. It can be seen that MCP, SCC and PTR derived from ICA decomposition (the first row) closely resemble corresponding tracts in the JHU atlas (the second row), with a Dice similarity of 0.81 (for MCP), 0.58 (for SCC) and 0.35 (for PTR) between the two maps. Although the JHU atlas is derived from DTI data, which represents the structural architecture of WM, our results from fMRI data demonstrate that these functional structures of WM match the anatomical architecture well, confirming a strong relationship between BOLD signals and DTI tractography.

More details of ICs for different orders (from 24 to 50) are provided in the supplementary materials (Fig. S3). It can be seen that more detailed separations of components showing correlated BOLD variations are obtained with a higher-dimensional ICA decomposition.

### 3.3. Symmetry of functional structures in white matter in a resting state

Several components were found to be paired bilaterally in the resting brain, as shown in Fig. 4. Spatial maps of these ICs superimposed on $T_1$ images and their coordinates are provided in Fig. S4 and Table S1. These components correspond to tracts in the JHU atlas including the posterior limb of the internal capsule (PLIC), anterior corona radiation (ACR), superior corona radiation (SCR), posterior corona radiation (PCR), and superior longitudinal fasciculus (SLF). It can be seen that one pair of tracts in the JHU atlas may correspond to two or more pairs of ICs derived by ICA decompositions, such as PLIC. The findings demonstrate that functional structures identified as sharing common patterns of spontaneous fluctuations in BOLD signals in a resting state, as detected by ICA, are consistent with specific tracts depicted in the JHU atlas that are derived from DTI, and these sub-structures are located symmetrically in bilateral WM tracts.

### 3.4. Functional connectivity between components in white matter in a resting state

We computed mean correlations between IC components by averaging the IC correlations of individual subjects, and found two groupings of correlated BOLD signals in WM. There is a clear anti-correlation between the two patterns, as indicated by the large cluster of blue elements in Fig. 5. The first pattern captures ICs that include MCP, pontine crossing (PC), PLIC, cerebral peduncle (CP), CST and SCC which are situated in and around the brain stem (termed here the synchronized brain stem systems). The second pattern contains some ICs that include PTR, SLF, ACR SCR and PCR, which are mainly located in the occipital lobe and involve areas related to higher order cognition (termed as the synchronized higher order cognition system including vision).

To further demonstrate coordinated patterns between components, the time courses of one pair of ICs (IC #19 and IC #24) are presented in Fig. 6. Although they are separated by a large spatial distance, their time courses are similar, with correlation coefficient of 0.59. It can be seen that IC #19 is located in the ACR (the peak value of IC #19 falls in ACR according to the JHU atlas and the software MRIcron), and IC #24 is in the optic radiation (Mori et al., 2008), the former of which is densely connected with the inferior frontal gyrus involved in visual processing (Takahashi et al., 2013) and the latter links directly to the visual cortex. We infer that those components in synchrony with the optic radiation define a

visual-related coactivation pattern, in which they share common baseline fluctuations, suggesting there may be general temporal oscillation patterns in WM across subjects.

The correlations between ICs represent a synchronous variation between BOLD signals, and reveal patterns of connectivity consistent with anatomical and functional relationships. For example, clusters of positive correlations correspond to coordination of information among WM networks, whereas the interpretation of negative correlations between the brain stem and vision-related neural activity is as yet unclear.

## 4. Discussion and conclusion

In this study, well-established ICA methods were applied to BOLD signals in WM during a task and at rest, to detect functional changes, to reveal functional structures and to explore functional connectivity within fMRI WM data. We first applied ICA to images produced by a finger movement task, and an IC evoked by the stimulus was robustly found. The time course of the IC was consistent with the task waveform. For left finger movements, WM signal changes were identified in the right corticospinal tract and in the left cerebellar peduncle, and were especially stronger in the right corticospinal tract than in the left. For right finger movements, WM signal changes were identified in the left corticospinal tract and in the right cerebellar peduncle, and were especially stronger in the left corticospinal tract than in the right. Overall, stronger functional changes were detected in the contralateral bundle of the corticospinal tract and in the ipsilateral bundle in the cerebellar peduncle, consistent with previous reports (Biswal et al., 1995; Ding et al., 2018), which demonstrates that functional changes in WM BOLD signals during a motor task can be detected by ICA.

We compared the response time series of voxels in single ICs in WM and GM, averaging across 12 subjects performing a left motor task, and found that the mean BOLD signal was substantially higher in GM than that in WM; but the standard deviation of GM was also larger than that in WM, so that the mean SNR across 12 subjects was lower in GM than that in WM, which agrees with our previous work (Huang et al., 2018). There was little measureable difference in time delays in motor voxels between WM and GM.

Second, ICA was applied to the WM BOLD data acquired from 30 subjects in a resting state to identify component structures that show co-activation time courses. Independently, we also extracted the major co-varying structures in the resting brains of 100 subjects taken from the HCP data. The results of these two separate experiments were consistent and demonstrated that functional architectures derived using ICA are reproducible across datasets and largely agree with the WM tracts in the JHU atlas (Mori et al., 2008). We also found symmetrical pairs of co-activation structures, which indicates there are bilateral functionally coupled variations in WM at rest.

Finally, functional connectivity derived from resting state temporal correlations among different ICs were quantified to explore resting state co-ordination of neural activity across WM regions. We found that there are two distinct patterns of functional correlations within WM, and the two patterns exhibit anti-correlation properties between each other, suggesting a type of co-ordination of BOLD signals across WM (Shine et al., 2019; Zhang et al., 2018).

The two distinct patterns of functional correlations are consistent with the presence of two different dominant patterns of oscillations in WM BOLD signals.

To minimize potential signal contaminations from nearby structures, the WM and GM volumes are confined within tightly thresholded masks (>0.8), which are created by SPM for each individual subject. Spatial smoothing with a small Gaussian kernel (FWHM = 4 mm) is performed separately within the WM volumes for each subject only after segmentation. Note that we examined individual WM masks and have made sure no subjects included obvious GM. In GIFT, a group mask is calculated using all subjects' masks by Boolean AND operations. Individual components of back-reconstruction were computed using the aggregate mixture matrix and the original input data. Because the input data contain only WM, individual components of back-reconstruction based on the input data will not introduce GM signals.

To test the repeatability of the reconstruction of functional structures in WM, ICs were derived from both CHCP and HCP datasets using identical procedures and parameters. To evaluate the impact of the number of components on the ICA outcome, the number of components was set from 16 to 50, and we observed that some components were very similar between the two separate datasets. The most representative and stable components are presented in Fig. 2 and Fig. S2, which agree well with WM tracts in the JHU atlas. Spatial map details of ICs for different orders (from 24 to 50) are provided in the supplementary materials (Fig. S3).

Our ICA results of resting state networks in segmented GM regions alone identified several networks consistent with previous results, including auditory, somatosensory, visual and DMN (Smith et al., 2009), giving confidence that our analysis methods were applied correctly. The results of ICA with GM regions alone for 30 subjects in a resting state are provided in Fig. S6, which shows that most networks are consistent with those reported in previous literatures (Smith et al., 2009; Allen et al., 2011).

### 4.1. Comparison with previous work

In our previous work, we demonstrated that BOLD signals in specific WM tracts in a resting state showed significant correlations with specific GM regions, and relevant WM tracts show BOLD increases in response to a specific stimulus (Ding et al., 2018). We also detected WM activations using a frequency spectral analysis of BOLD signal fluctuations evoked by visual stimuli administered with a well-defined frequency, and found regional distributions of the WM activations are consistent with fibers reconstructed using DTI (Huang et al., 2018). In both the above works, functional signal changes in WM were detected using a frequency spectrum analysis, in which signals at the fundamental stimulus frequency are considered to reveal activity-related changes. That approach relies on detecting the responses of BOLD signals to stimuli with a well-defined, known frequency, which is generally not applicable to resting state data because spontaneous fluctuations in resting conditions are not centered around a specific frequency. This limitation is overcome by the present work since ICA does not rely on prior knowledge on response frequencies – it is a data-driven method and allows us to be agnostic regarding the exact form of response (Calhoun et al., 2009), which is the

main difference between this work and our previous work (Ding et al., 2018; Huang et al., 2018).

ICA has been employed earlier by Marussich et al., who analyzed fMRI data acquired from human subjects both in a resting state and during naturalistic scene perception. The study was focused on the functional reorganization of WM structures, particularly in the optic tracts, resulting from a steady-state stimulation, and found stronger synchronization within the optic tracts and significant interactions with cortical visual networks (Marussich et al., 2017). Another work of similar flavor by Peer et al. classified WM voxels into distinct networks by K-means clustering (Peer et al., 2017), which was performed on the basis of functional connectivity. Compared to the clustering approach, which relies on signal correlations for clustering rather than assuming signal independence, our study uses a combination of PCA and ICA to achieve clustering by imposing a strong constraint of signal independence on the resulting components (Calhoun et al., 2001), similarly to Marussich et al. It is recognized that the work by Peer et al, as well as that by Marussich et al, share similar technical concepts with our work, all of which are data driven WM parcellations, but this work extends the earlier works by deriving WM functional structures in the entire brain from co-activation patterns, which largely agree with JHU atlas, and characterizing functional connectivity among the WM tracts, which further reveals that there are two dominant patterns of signal oscillations in WM functional activity.

### 4.2. Contributions of this work

Our study demonstrates that WM functional signal changes evoked by motor tasks are detectable using ICA without prior information on the task or brain activity such as seed definitions or stimulus waveforms, and we found that the amplitudes of activated voxels in GM are greater than in WM. Symmetrical functional structures identified using ICA are consistent with WM tracts derived from DTI. Analysis of functional connectivity within WM functional structures averaged over all subjects demonstrates that there are two distinct functional patterns of BOLD signal changes in WM, and the two patterns show anti-correlation from each other.

### 4.3. Limitations

One notable drawback of ICA is that criteria for selecting the number of components is not well defined, the number of desired components may affect the outcome, and the optimal number may be application dependent. To explore the appropriate number of components for our datasets, we studied ICA decompositions increasing from 24 to 50 components, details of which are provided in Fig. S3. The ICs found were nearly identical from the two separate datasets (CHCP and HCP). However, when extracting a larger number of ICs from resting fMRI data, more functional sub-structures are identified. Of note, some distinct functional components, including the MCP, CST, CP and PC, persist and show similar patterns regardless of the number of ICs, while some other functional components such as the PTR and PLIC are split into sub-networks with higher-order ICA. Each component represents a co-activated organization within WM voxels that shares similar temporal fluctuations, which may be defined as a functional network in WM just like those defined in GM. Some of the functional structures exhibit distinct neural functions, for instance, the

PTR (including the optic radiation), which could be defined as the visual network in WM, and the MCP and CST related to motor function could be defined as the motor network. But other structures need further studies to clarify their functionality. A number of RSNs were found in WM using ICA of fMRI signals, but more efforts are still needed to classify and interpret these networks.

Finally, we would like to point out that the similarity between the functional structures derived by ICA and WM tracts from the JHU atlas was only visually assessed in this work, except MCP, SCC and PTR. To test the validity of the correspondence established visually, we randomly shuffled the voxels within WM 1000 times before the data were fed into the ICA algorithm, and found that the expected functional structures disappeared. It is recognized that the visual assessments performed here are qualitative in nature, and therefore more statistically rigorous tests of significance of the overlaps between functional structures and corresponding WM tracts are needed in future studies.

In summary, in this study ICA was used to decompose fMRI WM data into multiple components by maximizing their statistical independence, in order to detect BOLD signal changes elicited by motor tasks, to discover hidden spatiotemporal structures that show co-varying behaviors, and to explore function connectivity features within WM. Our findings demonstrate that functional signal changes and functional structures in WM can be detected and identified; the functional connectivity within WM indicates that there exist two distinct functional patterns of BOLD signal changes across widespread brain networks. Future work could further explore the temporal flow of signal changes within WM BOLD signals and characterize the time-frequency features of the spontaneous fluctuations from WM fMRI. More generally, we hope that this work will provide a platform for gaining insights into the origins and interpretations of BOLD signal changes in WM, their spatial structural organizations, and their measured apparent functional connectivity.

## Supplementary Material

Refer to Web version on PubMed Central for supplementary material.

## Acknowledgments

This work was supported by the National Natural Science Foundation of China (81727808, 81790651, 11771115, 11271106), the Youth Foundation of Hebei Province Educational Department (QN2016169), the Scientific Research Foundation for the Returned Overseas Chinese Scholars in Hebei Province (606999919029), Advanced Talents Incubation Program of Hebei University (801260201075, 521000981324), Hebei University supercomputer center and the Post-doctoral Research Foundation of Hebei University. Studies and efforts at Vanderbilt University were supported by NIH grant R01 NS093669 and R01 NS113832 awarded by NINDS to John C. Gore.

## References

Ogawa S, Lee TM, Kay AR, Tank DW, 1990 Brain magnetic resonance imaging with contrast dependent on blood oxygenation. Proc. Natl. Acad. Sci. USA 87 (24), 9868–9872. [PubMed: 2124706]

Biswal B, Zerrin Yetkin F, Haughton VM, Hyde JS, 1995 Functional connectivity in the motor cortex of resting human brain using echo-planar mri. Magn. Reson. Med 34 (4), 537–541. [PubMed: 8524021]

Fox MD, Raichle ME, 2007 Spontaneous fluctuations in brain activity observed with functional magnetic resonance imaging. Nat. Rev. Neurosci 8 (9), 700–711. [PubMed: 17704812]

Gonzalez-Castillo J, Handwerker DA, Robinson ME, et al., 2014 The spatial structure of resting state connectivity stability on the scale of minutes. Front. Neurosci 8, 138. [PubMed: 24999315]

Zhang D, Raichle ME, 2010 Disease and the brain's dark energy. Nat. Rev. Neurol 6 (1), 15. [PubMed: 20057496]

Lee MH, Smyser CD, Shimony JS, 2013 Resting-state fMRI: a review of methods and clinical applications. Am. J. Neuroradiol 34 (10), 1866–1872. [PubMed: 22936095]

Fox MD, Greicius M, 2010 Clinical applications of resting state functional connectivity. Front. Syst. Neurosci 4, 19. [PubMed: 20592951]

Raichle ME, MacLeod AM, Snyder AZ, et al., 2001 A default mode of brain function. Proc. Natl. Acad. Sci. USA 98 (2), 676–682. [PubMed: 11209064]

Buckner RL, Andrews-Hanna JR, Schacter DL, 2008 The brain's default network. Ann. N. Y. Acad. Sci 1124 (1), 1–38. [PubMed: 18400922]

Greicius M, 2008 Resting-state functional connectivity in neuropsychiatric disorders. Curr. Opin. Neurol 21 (4), 424–430. [PubMed: 18607202]

Ding Z, Newton AT, Xu R, et al., 2013 Spatio-temporal correlation tensors reveal functional structure in human brain. PLoS One 8 (12), e82107. [PubMed: 24339997]

Ding Z, Huang Y, Bailey SK, et al., 2018 Detection of synchronous brain activity in white matter tracts at rest and under functional loading. Proc. Natl. Acad. Sci. USA 115 (3), 595–600. [PubMed: 29282320]

Marussich L, Lu KH, Wen H, Liu Z, 2017 Mapping white-matter functional organization at rest and during naturalistic visual perception. Neuroimage 146, 1128–1141. [PubMed: 27720819]

Peer M, Nitzan M, Bick AS, Levin N, Arzy S, 2017 Evidence for functional networks within the human brain's white matter. J. Neurosci 37 (27), 6394–6407. [PubMed: 28546311]

Basser PJ, Mattiello J, LeBihan D, 1994 MR diffusion tensor spectroscopy and imaging. Biophys. J 66 (1), 259–267. [PubMed: 8130344]

Ding Z, Xu R, Bailey SK, et al., 2016 Visualizing functional pathways in the human brain using correlation tensors and magnetic resonance imaging. Magn. Reson. Imaging 34 (1), 8–17. [PubMed: 26477562]

Gore JC, Li M, Gao Y, et al., 2019 Functional MRI and resting state connectivity in white matter-a mini-review. Magn. Reson. Imaging 63, 1–11. [PubMed: 31376477]

Grajauskas LA, Frizzell T, Song X, D'Arcy RC, 2019 White matter fMRI activation cannot be treated as a nuisance regressor: Overcoming a historical blind spot. Front. Neurosci 13, 1024. [PubMed: 31636527]

Mazerolle EL, D'Arcy RC, Beyea SD, 2008 Detecting functional magnetic resonance imaging activation in white matter: interhemispheric transfer across the corpus callosum. BMC Neurosci 9 (1), 84. [PubMed: 18789154]

Gawryluk JR, Brewer KD, Beyea SD, D'arcy RC, 2009 Optimizing the detection of white matter fMRI using asymmetric spin echo spiral. Neuroimage 45, 83–88. [PubMed: 19084071]

Gawryluk JR, Mazerolle EL, Brewer KD, Beyea SD, D'Arcy RC, 2011 Investigation of fMRI activation in the internal capsule. BMC Neurosci 12 (56), 1–7. [PubMed: 21208416]

Fabri M, Polonara G, 2013 Functional topography of human corpus callosum: an FMRI mapping study. Neural Plast 2013, 1–15.

Wu X, Yang Z, Bailey SK, et al., 2017 Functional connectivity and activity of white matter in somatosensory pathways under tactile stimulations. Neuroimage 152, 371–380. [PubMed: 28284801]

Huang Y, Bailey SK, Wang P, et al., 2018 Voxel-wise detection of functional networks in white matter. Neuroimage 183, 544–552. [PubMed: 30144573]

Li M, Newton AT, Anderson AW, Ding Z, Gore JC, 2019 Characterization of the hemodynamic response function in white matter tracts for event-related fMRI. Nat. Commun 10 (1), 1140. [PubMed: 30850610]

Calhoun VD, Adali T, Pearlson GD, Pekar JJ, 2001 A method for making group inferences from functional MRI data using independent component analysis. Hum. Brain Mapp 14 (3), 140–151. [PubMed: 11559959]

Calhoun VD, Liu J, Adalı T, 2009 A review of group ICA for fMRI data and ICA for joint inference of imaging, genetic, and ERP data. Neuroimage 45 (1), S163–S172. [PubMed: 19059344]

Calhoun VD, Adali T, Pearlson G, Pekar JJ, 2001 Spatial and temporal independent component analysis of functional MRI data containing a pair of task-related waveforms. Hum. Brain Mapp 13 (1), 43–53. [PubMed: 11284046]

McKeown MJ, Jung T-P, Makeig S, et al., 1998 Spatially independent activity patterns in functional MRI data during the Stroop color-naming task. Proc. Natl. Acad. Sci. USA 95 (3), 803–810. [PubMed: 9448244]

Biswal BB, Ulmer JL, 1999 Blind source separation of multiple signal sources of fMRI data sets using independent component analysis. J. Comput. Assist. Tomogr 23 (2), 265–271. [PubMed: 10096335]

Beckmann CF, DeLuca M, Devlin JT, Smith SM, 2005 Investigations into resting-state connectivity using independent component analysis. Philos. Trans. R. Soc. B: Biol. Sci 360 (1457), 1001–1013.

Smith SM, Fox PT, Miller KL, et al., 2009 Correspondence of the brain's functional architecture during activation and rest. Proc. Natl. Acad. Sci. USA 106 (31), 13040–13045. [PubMed: 19620724]

Smith SM, Miller KL, Moeller S, et al., 2012 Temporally-independent functional modes of spontaneous brain activity. Proc. Natl. Acad. Sci. USA 109 (8), 3131–3136. [PubMed: 22323591]

Van Essen DC, Smith SM, Barch DM, et al., 2013 The WU-Minn human connectome project: an overview. Neuroimage 80, 62–79. [PubMed: 23684880]

Mori S, Oishi K, Jiang H, et al., 2008 Stereotaxic white matter atlas based on diffusion tensor imaging in an ICBM template. Neuroimage 40, 570–582. [PubMed: 18255316]

Shine JM, Breakspear M, Bell PT, et al., 2019 Human cognition involves the dynamic integration of neural activity and neuromodulatory systems. Nat. Neurosci 22 (2), 289. [PubMed: 30664771]

Bell AJ, Sejnowski TJ, 1995 An information-maximization approach to blind separation and blind deconvolution. Neural Comput 7 (6), 1129–1159. [PubMed: 7584893]

Petersen K, Hansen LK, Kolenda T, Rostrup E, Strother S, 2000 On the independent components of functional neuroimages. In: Proceedings of the Third International Conference on Independent Component Analysis and Blind Source Separation, pp. 615–620.

Bürgel U, Amunts K, Hoemke L, et al., 2006 White matter fiber tracts of the human brain: three-dimensional mapping at microscopic resolution, topography and inter-subject variability. Neuroimage 29, 1092–1105. [PubMed: 16236527]

Takahashi E, Ohki K, Kim D-S, 2013 Dissociation and convergence of the dorsal and ventral visual working memory streams in the human prefrontal cortex. Neuroimage 65, 488–498. [PubMed: 23063444]

Zhang H, Watrous AJ, Patel A, Jacobs J, 2018 Theta and alpha oscillations are traveling waves in the human neocortex. Neuron 98 (6), 1269–1281 e1264. [PubMed: 29887341]

Allen EA, Erhardt EB, Damaraju E, et al., 2011 A baseline for the multivariate comparison of resting-state networks. Front. Syst. Neurosci 5, 1–23. [PubMed: 21347218]

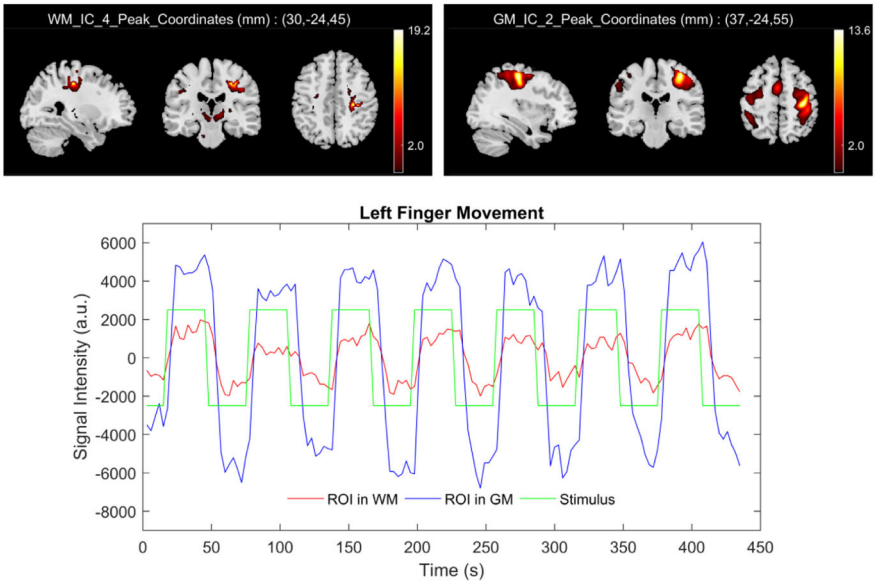


(a)

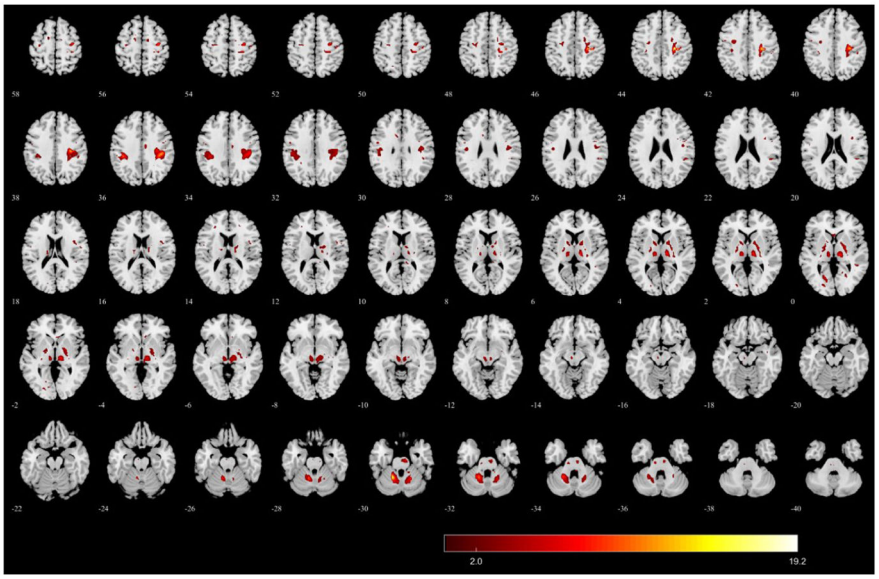


(b)

**Fig. 1.**

Spatial maps and time courses from ICA averaged across 12 subjects for left finger movement task (the right brain is on the right side). a) Three selected orthogonal slices of the ICA components #4 in WM (upper left) and #2 in GM (upper right) superimposed onto $T_1$ weighted images in MNI space; the mean time series of the activations shown in the same WM and GM components ($Z$-scores $>3$) are shown below (WM: red; GM: blue; stimulus: green), and the mean fMRI data within the IC maps were removed for display; b) Axial slices (−40–58) showing spatial maps of ICA component #4 in WM in MNI space. All spatial maps were thresholded at $Z > 2$ ($p < 0.05$), and the color bar denotes Z-scores.

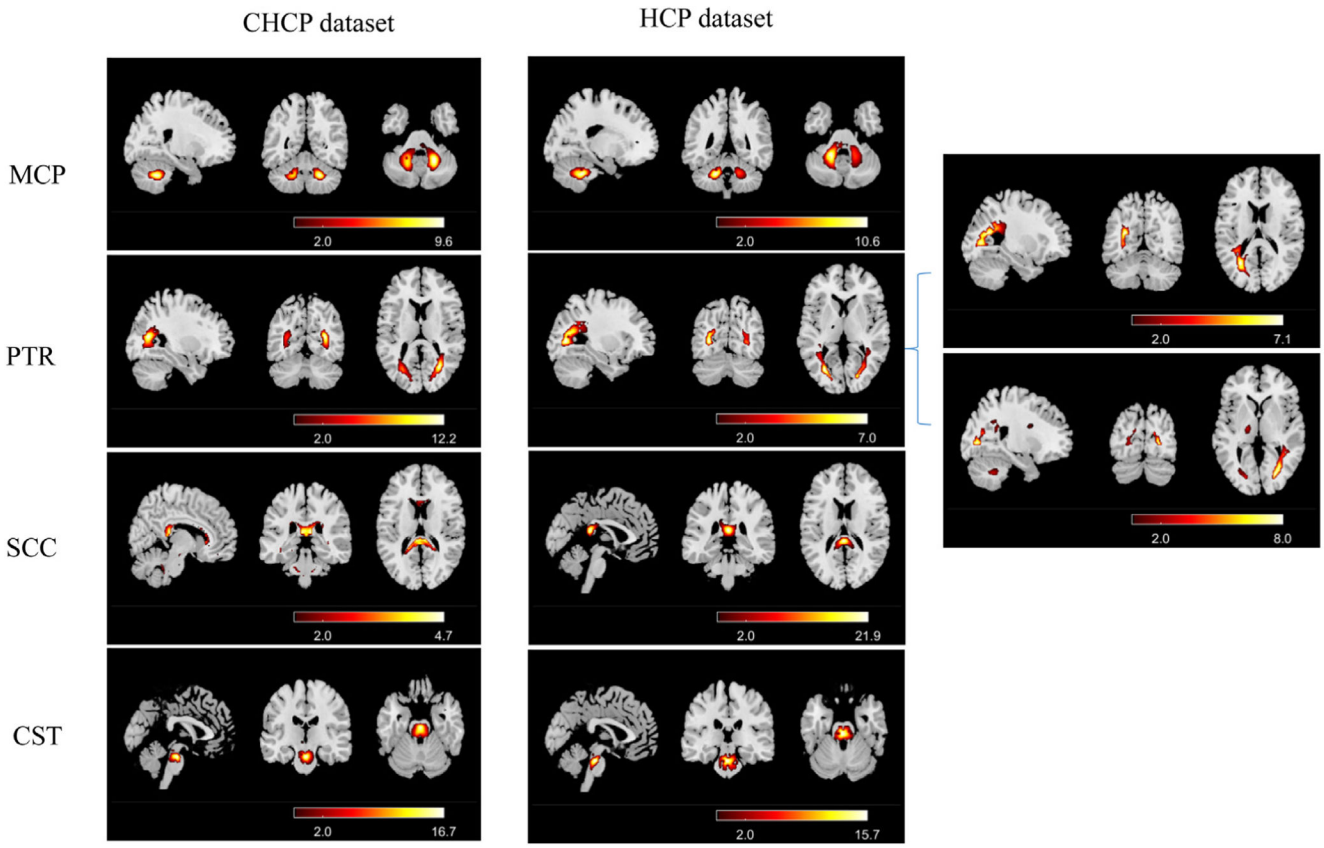


**Fig. 2.**

Functional structures within WM from the 30-subject CHCP database and the 100-subject HCP dataset using ICA (the order of ICA decomposition here is 24). This figure shows the three most informative orthogonal slices for each functional component. All spatial maps were thresholded at $Z > 2$ ($p < 0.05$), and the color bar denotes Z-scores.

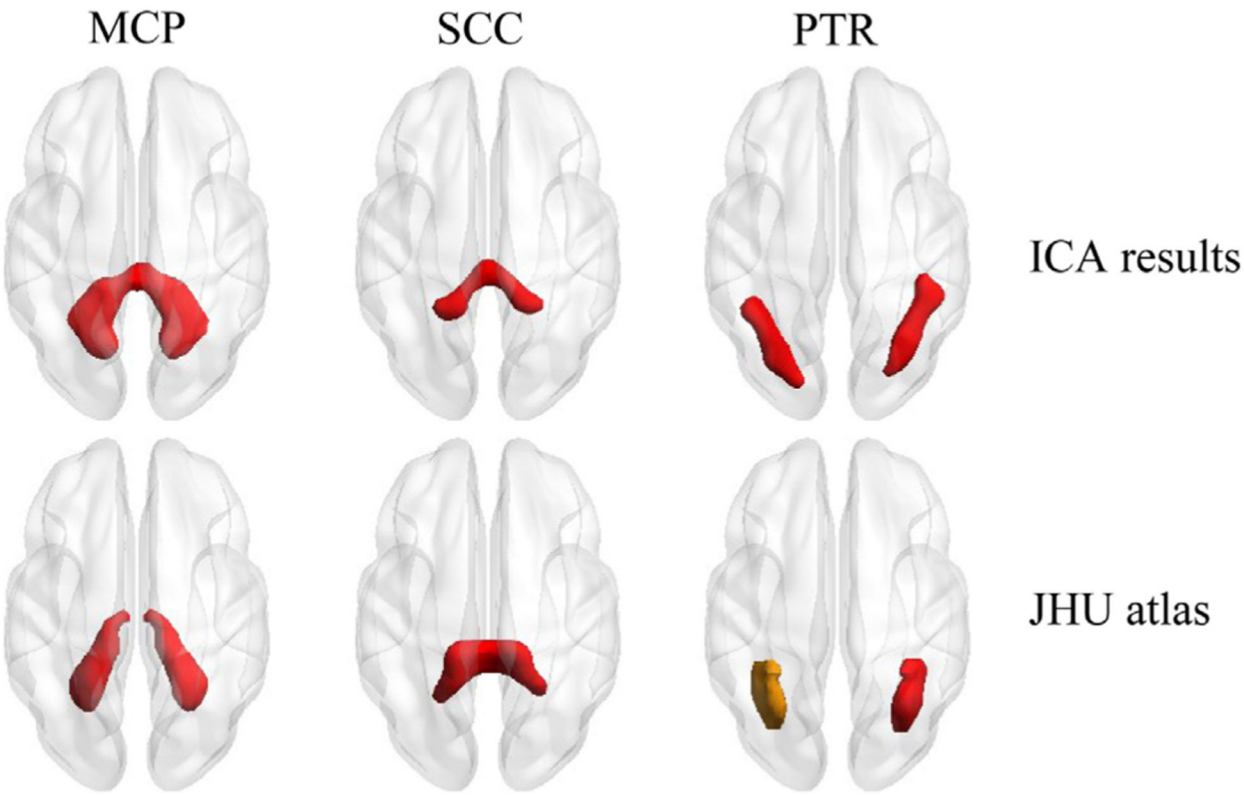


**Fig. 3.**

Comparisons of WM structures derived from ICA results of fMRI (the first row, ICA decomposition from BOLD data) and JHU atlas from DTI (the second row, WM tracts from JHU atlas).

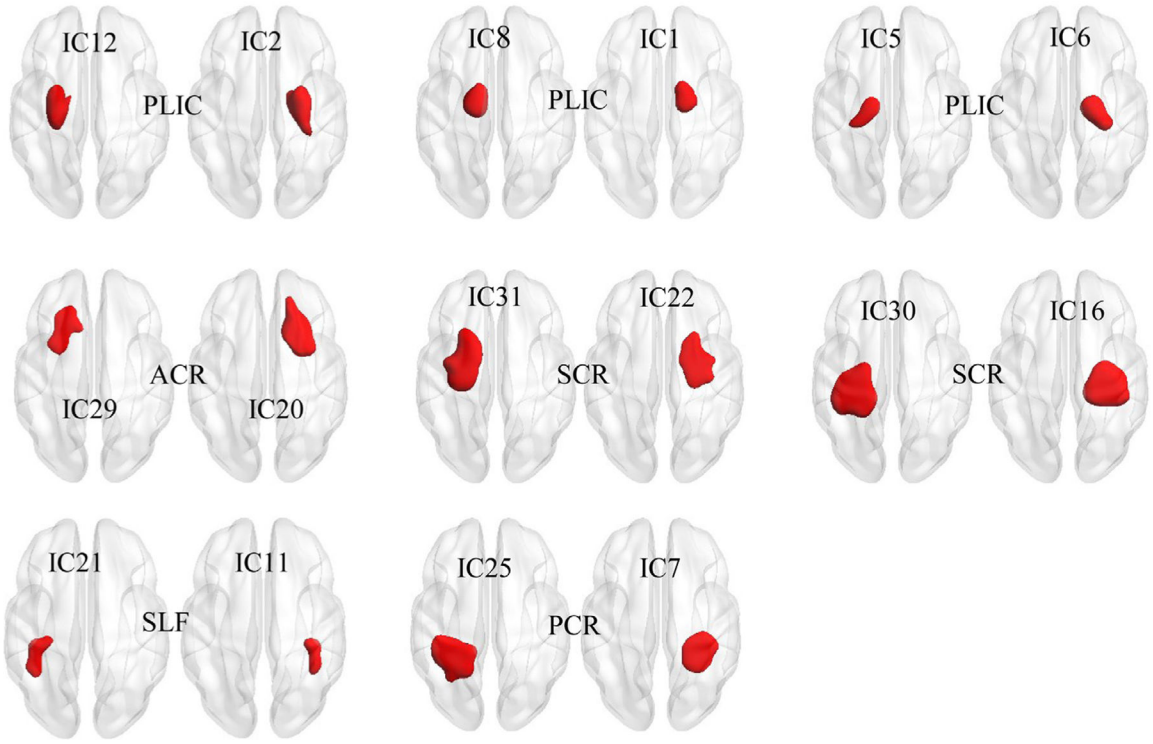


**Fig. 4.**

Symmetric functional structures in white matter derived from ICA; more details of components are presented in supporting information (Fig. S4 and Table S1).

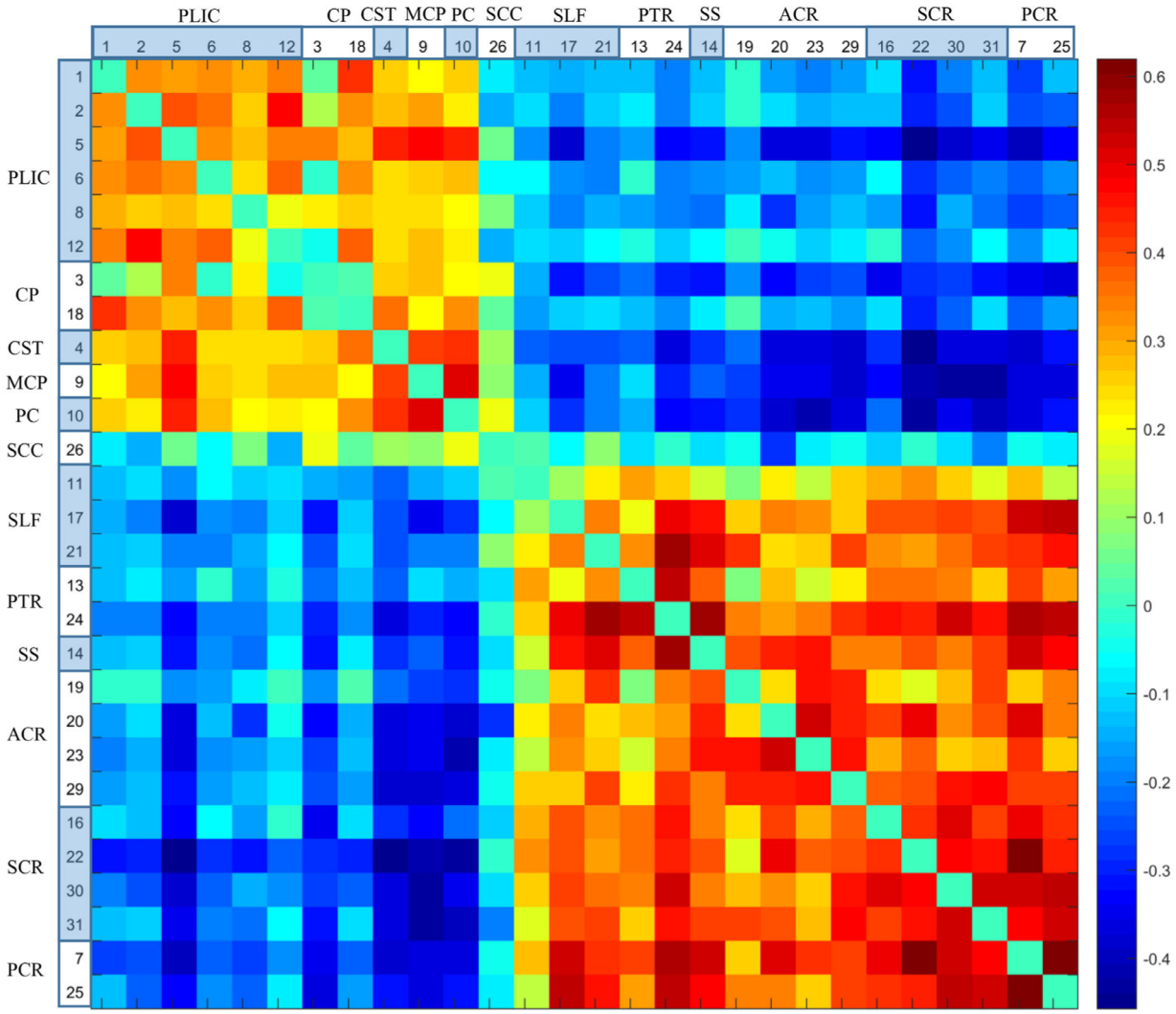


**Fig. 5.**

Functional connectivity within WM structures. ICs are grouped based on their anatomical properties and correlation coefficients, and include posterior limb of internal capsule (PLIC), cerebral peduncle (CP), corticospinal tract (CST), middle cerebellar peduncle (MCP), pontine crossing (PC), splenium of corpus callosum (SCC), superior longitudinal fasciculus (SLF), posterior thalamic radiation (PTR), sagittal striatum (SS), anterior corona radiation (ACR), superior corona radiation (SCR) and posterior corona radiation (PCR). The spatial maps of these ICs are provided in supplementary materials (Fig. S5).

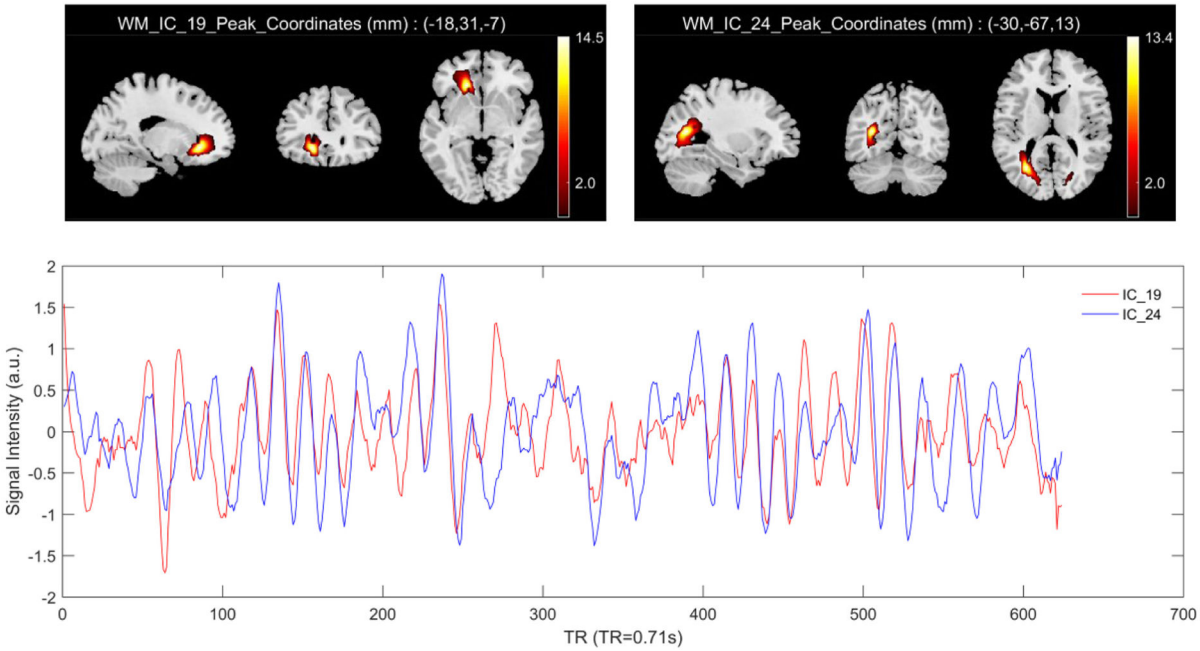


**Fig. 6.**

Spatial maps and time courses of one pair of ICs (IC #19 and IC #24). All spatial maps were thresholded at $Z > 2$ ($p < 0.05$), and the color bar denotes Z-scores.